

Optimization of Hollow Core Slab Strength Based on SFRC Orientation

Abdulaziz Boushi^{1*} , Sepanta Naimi² 

Faculty of Engineering and Architecture, Department of Civil Engineering, Altınbaş Üniversitesi, Bağcılar 34217, İstanbul, Turkey

Corresponding Author Email: 203724525@ogr.altinbas.edu.tr



<https://doi.org/10.18280/mmep.100112>

ABSTRACT

Received: 30 September 2022

Accepted: 16 December 2022

Keywords:

SFRC, SFRC Orientation, hollow core, structural response, hollow core slab, finite element analysis

The construction industry has been broadly developed and improved over the last decades. One of the functional innovations in this sector is the employment of steel fibers. This work assesses the impacts of using Steel Fiber Reinforced Concrete (SFRC) on the properties of hollow-core slabs. The hollow core slab (HCS) is considered in this research. Also, this study explored the influence of utilizing some SFRC fractions on the characteristics of hollow-core slabs. Four case studies were addressed, including (A) Conventional concrete, (B) Concrete with Type 1 SFRC, (C) Concrete with Type 2 of SFRC with a ratio of 0.5%, and (D) Concrete with Type 2 with a portion of 1%. ANSYS software package was used to guide numerical analysis and modeling of HCS and identify major parameters that affect the HCS performance with the help of Finite Element Analysis (FEA). Depending on the numerical results, it was found that using SFRC between 0.5% and 1% in concrete tubes tested numerically provided significant rates of durability, minimized deflection, and enhanced the mechanical behavior of concrete. Furthermore, the work outcomes confirmed that optimum displacement was attained when the SFRC ratio was 1.5%, corresponding to load values of 25 kN to 200 kN. Besides, the findings affirmed that using the first type of SFRC accomplished a considerable decline in the deflection of concrete. Deflection reduction ratios of 4.16% and 6.23% were obtained after adding the first and second types of SFRC into the reinforced hollow concrete core, respectively. Meanwhile, adding the first and second types of SFRC into non-reinforced hollow concrete core accomplished a reduction portion of 12.2% and 20.39%, respectively.

1. INTRODUCTION

The installation of flooring systems made of hollow slab concrete is a common practice in a lot of different nations [1]. The use of hollow core modules in building construction is becoming increasingly widespread, notably as components for the floors and roofs of buildings [2-4]. It is possible to achieve rapid construction timeframes, a high degree of quality, and a steady reduction in the structure's weight, which enables manufacturers to cover longer spans [4, 5]. It is common practice to manufacture Hollow-Core HCSs with a thickness ranging from 100 to 400 mm and a width ranging from 900 to 1,250 mm [6, 7]. The span can go up to 18 meters [7, 8]. Recent findings from several studies have suggested that including fibers in concrete structures might increase the performance of the buildings, even though concrete is a material that is brittle and has poor tensile strength. The ability of fibers to transmit stresses across a fracture is the primary advantage of using them in concrete [7]. It helps improve the toughness and flexibility of the concrete while increasing its capacity to absorb impact forces [8]. High tensile strength fibers such as steel, carbon, glass, aramid, and other similar materials produce fiber reinforcement. The influence of shear pressures is one of the primary obstacles that must be overcome in the structural design process [9]. There must be sufficient shear strength at the interface for the composite action. The joint's horizontal and vertical shear strengths

between adjacent hollow core units must be sufficiently high to transmit the forces caused by flat diaphragm action and the load-sharing of concentrated loads [8, 9]. Within the discontinuity zone, the transfer mechanism of shear forces is to blame for this phenomenon, which also occurs there. These shear stresses are caused not only by gravity loads but also by unbalanced moments and movement resulting from occurrences like earthquakes and strong winds [10]. Figure 1, derived from the tests carried out by Herlihy and Park, depicts the failure of the hollow-core unit as presented in Figure 1 below [10].



Figure 1. Failure of Hollow-Core in the 1994 Northridge earthquake [8]

1.1 Problem statement

The geometrical and mechanical properties of fiber can change based on their impacts, and these changes endow concrete with a set of features that are not seen anywhere else. The dependability of fiber-reinforced concrete is based on a range of parameters, including the orientation of the fibers, the type of fibers used, and the percentage of fibers utilized. The workability of the mixture deteriorated whenever the number of particles increased to their size, which was more than 5 millimeters. The aspect ratio, often known as l/d , is another vital component that should not be overlooked. It considerably influences the fibers' flexibility, affecting their capacity to deal with them. The fibers' workability decreases to the degree that the aspect ratio increases, and this decrease is proportional to the rise. Fibers can prevent cracking and promote flexibility and tensile strength in a material. Steel rebars and steel fiber reinforced concrete, often known as steel fiber reinforced concrete (SFRC) [11-15], are both options for the structural reinforcing of concrete components. This method makes it possible to avoid the brittle fracture behavior that is inherently present in concrete, in addition to providing other benefits, including the prevention of cracking due to initial shrinkage and endogenous concrete shrinking at an early age. When shear stresses are present, using Fibers Reinforced Concrete (FRC) can eliminate the need for conventional rebar. That results in savings in terms of the amount of time spent sitting, the amount of labor force required [16], the weight of the finished product, and a reduction in overall production costs [17-22].

1.2 Objectives and scope

Experiments will be conducted to determine how fibers influence the residual strength of HCS to accomplish the following goals:

- (1) To investigate the differences in shear resistance between the various steel fiber reinforced concrete (FRC).
- (2) To explore the optimum properties of steel fibers to maximize the shear capacity of hollow core slab HCS.

2. TYPES OF FIBERS FOR REINFORCED CONCRETE

By substituting cast-in-sit reinforced concrete for precast specimens, the construction procedure for precast specimens has been improved. It is owing to these essential benefits, which include superior specimen quality and affordable, conventional manufacturing processes used in factories [13, 23, 24].

Fibers Reinforced Concrete (FRC) is based on more than half a century's expertise with the implementation of steel fibers in a concrete matrix in a random arrangement. In recent years, several additional forms of fiber have demonstrated that they are suitable for use in substantial structural parts and have comparable performance [15].

As presented in Figure 2 the classification of natural fibers. They are divided into two subcategories: vegetable origin and Animal Origin. Vegetable origin is further subdivided into four categories: wood fibers, hast fibers, leaf fibers, and leaf fibers. Animal Origin is divided into two subcategories: wool and hair fibers and silk and other filaments. All of these fibers have different properties and are used in different objects as presented in Figure 2 below.

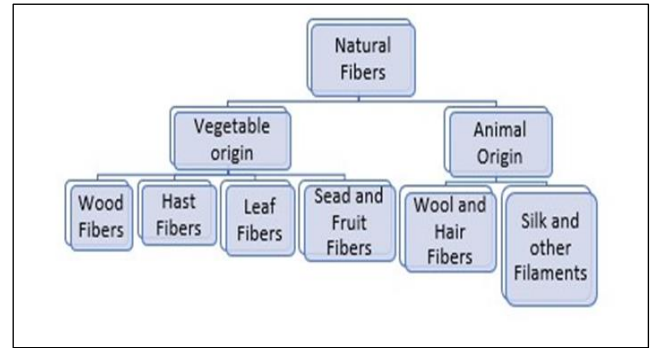


Figure 2. Natural fiber classification [20]

2.1 Polypropylene fiber reinforced concrete

The primary ingredient for polypropylene is monomeric C_3H_6 , a pure hydrocarbon. Polypropylene is made from this substance [17-19]. Polypropylene fibers have several desirable properties thanks to their polymerization process, high molecular weight, and fiber processing methods, which will be discussed in further depth below:

(A) The polymer molecule's structure exhibits excellent crystallinity and a hydrogen-bonding arrangement of its atomic constituents. Isotactic polypropylene is the name given to this material because of its highly ordered structure. Because they are chemically inert, the fibers are resistant to most chemicals [17]. Any chemical that does not break down the components of the concrete will not affect the fiber in any way. Concrete is always the first material to disintegrate when it comes into touch with more acidic substances [18].

(B) Because the hydrophobic surface does not absorb moisture from the cement paste, chopped fibers do not experience the same balling effect as other fibers when mixed.

(C) Polypropylene fibers have no requirement for any amount of water at all.

(D) Because of the orientation, the film is fragile in the lateral direction, which makes it easier for fibrillations to form. Therefore, the cement matrix can permeate the mesh structure between the individual fibrils, creating a mechanical link between the matrix and the fiber.



Figure 3. Polypropylene Fibers [17]

It can be inferred from Figure 3 that the shape of polypropylene fibers varied. The fibrillated polypropylene fibers were produced by the expansion of a plastic film, which was then cut into strips and sliced before being further processed [19].

2.2 Properties of polypropylene (Pp) fiber reinforced concrete

Compared to ordinary concrete mixes, FRC mixes often include a more significant amount of mortar volume. Because excessively long fibers tend to "ball" in the concrete mix and cause difficulties with workability, the aspect ratio of the fibers can only be between 100 and 200. In most cases, the fibers in the concrete are dispersed haphazardly. On the other hand, laying the concrete, which results in increased flexural and tensile strength, should be done in the opposite direction of the applied stress [1, 2]. For the fresh concrete to flow effectively and for the polypropylene (PP) fibers to be distributed equally throughout the mixture, there has to be a sufficient amount of compaction. The fibers in the newly mixed concrete shouldn't settle to the bottom and shouldn't float to the surface. The handling qualities of the wet mix, as well as its strength, water content, volumetric stability, and cement ratios, can be improved with the help of superplasticizers [5, 21, 25-28].

2.3 Typical crack pattern

The primary purpose of structural analysis is to determine how a structure will respond to a given activity. This activity might be a calamity of a different kind, like an earthquake, or it could be a structure of load caused by the weight of things like people, snow, and storms. Together, these masses are dynamic due to the structure's weight. The primary distinction between dynamic and static studies is whether or not the applied action accelerates appropriately relative to the structure's inherent frequency. Inertia forces may be ignored, and the assessment can be condensed to static analysis if a load is supplied gradually. A kind of structural analysis called structural dynamics shows how structures respond to dynamic loads [11].

Cracking in concrete is caused by a combination of factors, including mechanical loading and the characteristics of the surrounding environment. The stress mechanisms that cause concrete to break can be divided into two categories: when the concrete is in its plastic state and when the concrete has hardened. These stress mechanisms can also be differentiated according to whether they are caused by internal or external factors [1-3]. For instance, chemical reactions, thermal expansion, constraint, and overloading are all examples. The cracks themselves can range in size from microscopic fissures found on the inside to enormous fissures caused by the actions of exterior environmental elements [6, 7]. Even the smallest amount of negligence might produce discomfort in the concrete HCS pavement during the building process. Cracks might emerge in concrete Haus due to the strain caused by various elements like the introduction of water, seasonal temperature variations that induce expansion and contraction, and exposure to the sun. To calculate the theoretical capacity curve, you need to identify two different points: first, the width of the activated flange when the beams yield for the first time, and second, the width of the active flange when the super-assembly has reached its maximal plasticity. Within the shear span zone, it was possible to see diagonal cracks, as shown in Figure 4 and the sample HCS load-deflection response is shown in Figure 5. The primary oblique fracture continued to spread with the advancement of loading stages until shear failure occurred as presented in Figure 4 and Figure 5 below [3].



Figure 4. Mode of failure and cracks pattern of HCS [3]

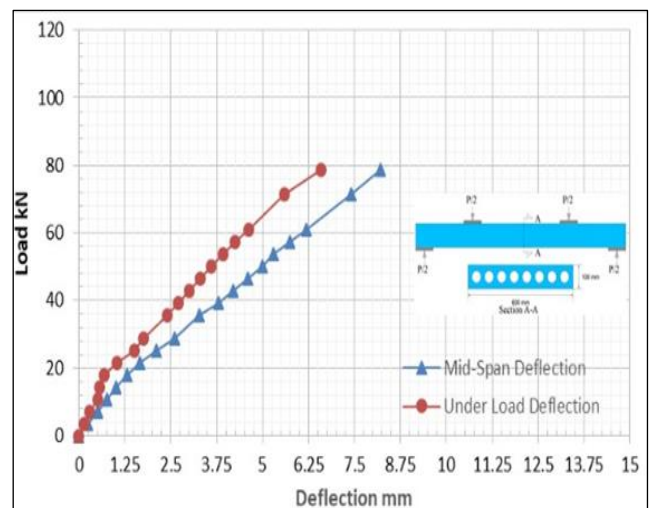


Figure 5. Sample of the load deflection response of HCS [3]

2.4 Ultimate load proposed equations

(I) Since punching shears have been around for many years, several codes have been written to provide designs and calculation requirements for punching shear capacity. Some examples of these codes include the following:

(II) The standards recommended by the British standard BS8110:1985 are comparable to what Regan suggested.

$$V_c = const \times (p \times f'c)^{\frac{1}{3}} \times (400)/(d)^{1/4} \quad (1)$$

(SI units) where d is the effective depth of HCS in mm.

(III) Nevertheless, the critical shear perimeters are shown to be rectangular and to be positioned $1.5d$ from the face of the column in the British standard BS8110:1985, and this is the case regardless of whether the column shape is circular or rectangular.

(IV) ACI 318-83 and CSA A23.3 84M: The punching perimeter in ACI 318-83 and CSA A23.3 84M is positioned at a distance of $d/2$ from the column face, and both of these standards compute the shear strength from the root of the concrete strength [2, 6].

$$(V) \quad V_u = 0.33 b_o d (f'c)^{1/2} \quad (2)$$

where, bo is the perimeter $d/2$ from the column face, d effective depth?

A contract with the Construction Industries Research and Information Association mandated that Regan establish an equation for determining punching shear capacity. Regan proposed a formula to assess the properties of a circular shear perimeter that was situated 1.25 from the face of circular columns and a rounded rectangular shear perimeter that was located 1.25 from the face of rectangular columns for the shear perimeter of the shear zone. This formula can be expressed as:

$$V_u = K_a K_{SC} K_S (p \times f'c) l/3 \times d (\Sigma c + 7.85d) \quad (3)$$

where,

V_u : ultimate Shear force.

K_a : 0.13 for concrete of normal density.

K_{SC} : $1.15 \times (4\pi \times \text{column area} / (\text{column perimeter})^2)^{1/2}$.

K_S : size effect term $(300/d)^{1/4}$ (SI units).

p : steel ratio.

$f'c$: compressive strength.

d : effective depth of HCS in mm.

Σc : the perimeter of the column.

(VI) Bazant and Cao focused on the size effects; also, a formula was suggested for calculating the punching shear:

$$v_u \frac{V_u}{D_p h} \quad (4)$$

$$v_c \text{ const } f'c \frac{(1 + 0.6 \frac{D_p}{h})}{(1 + \frac{h}{25d_{agg}})^{1/2}} \quad (5)$$

where, D_p diameter of punching, h HCS thickness, d_{agg} maximum aggregate size.

3. RESEARCH METHODOLOGY

The finite element method, often known as FEM [29-33], is an essential strategy for numerical analysis of a wide range of issues in civil engineering, in addition to other subfields of engineering. A significant portion of this investigation is focused on the effect of the hollow core's structure. The many numerical approaches and various computerized algorithms are utilized to solve and analyze issues that include a problem's structural and material components. The analysis of the consequences of these significant factors consists of many essential characteristics, such as the circle thickness and the material composite system [14, 16].

ANSYS is a comprehensive computer program for finite elements that can be used for various purposes and contains more than 180 types. Both static and dynamic analysis are within its scope of capability. Since well over twenty years ago, it has established itself as the top program for finite element analysis [16]. It is a highly unique and robust instrument that may be utilized in engineering to tackle various issues. The comprehensive finite element model of the hollow core structure was produced with the assistance of the procedures included in the ANSYS Finite Element software. Based on the ANSYS program's advice and by contrasting the analytical findings with experimental results of both changed and unmodified specimens, a mesh sensitivity analysis was conducted to establish the optimal mesh density [11]. The

numerical analysis of the system was built on top of this model. By using the 3-D model, it enables to replicate of the braces' uniaxial behavior, which is referred to as "tension alone."

Hollow core slabs are parts made of precast concrete with a cross-section that is always the same size [12]. They are made with single wires or prestressed strands with high tensile strength and are incorporated inside the element during manufacturing. These components are manufactured with our Extruder, slip former, and Wet Casting machine, which is cast in a single phase along a production bed without using any formworks. Hollow core slabs are highly developed structural components utilized worldwide due to their numerous benefits and the wide variety of contexts in which they may be used. As a result of their technical and financial qualities, they are currently considered one of the most well-known prefabricated pieces. Construction projects in the residential, commercial, and industrial sectors, as well as infrastructure development, make extensive use of hollow core slabs for flooring and wall panels.

3.1 Case studies description

In this research paper, Table 1 illustrates the methodology utilized to analyze the behavior of the hollow core upon the addition of the SFRC while subjected to various stressful circumstances. The first thing that needed to be done was to specify a concrete mix design based on the paper that Yousif Nassif Sabr and his colleagues published in (2019) for validation purposes.

Table 1. Concrete cubes test procedure

Test code	Concrete conditions	No of samples
ABD 1-1	Traditional concrete	6
ADB 1-2	concrete with SFRC type 1	6
ABD 2-1	concrete with SFRC type 2, v=0.5	6
ABD 2-2	concrete with SFRC type 2, V=1.0	6

Using the ANSYS simulation tool, the following phase is researching the influence of the kind of concrete used on hollow core slabs. The following is a description of the simulation program that can be found in Table 2.

Table 2. ANSYS simulation procedure for V= 0.5

Test code	Concrete conditions	SFRC volume
HBD 1-1	Traditional concrete	NON
HBD 1-2	Traditional concrete with SFRC	V=0.5
HDB 1-3	Reinforced concrete	V=0.5
HBD 1-4	Reinforced concrete with SFRC type 1	V=0.5

Table 3. ANSYS simulation procedure for V= 1.0

Test code	Concrete conditions	SFRC volume
HBD 1-1	Traditional concrete with SFRC type 1	V=1.0
HBD 1-2	Traditional concrete with SFRC type 2	V=1.0
HDB 1-3	Reinforced concrete with SFRC type 1	V=1.0
HBD 1-4	Reinforced concrete with SFRC type 2	V=1.0



Figure 6. Compression test results for traditional concrete and concrete with SFRC

Table 4. Properties for reinforced and concrete compressive stress

The 28 days compressive stress of concrete f'_c (MPa)	35.5
The 28 days compressive stress of concrete with SFRC fiber reinforced (type 1) f'_c (MPa)	38.45
The 28 days compressive stress of concrete with SFRC fiber reinforced (type 2) f'_c (MPa)	39.64

The primary objective of the experiments is to determine the compression resistance by utilizing various quantities of SFRC fibers as it is shown in Figure 6. After these tests has been accomplished, the concrete resistance will be applied to the ANSYS hollow core model to investigate the behavior and characteristics of hollow core slabs as it is shown in Tables 3 and 4 [15].

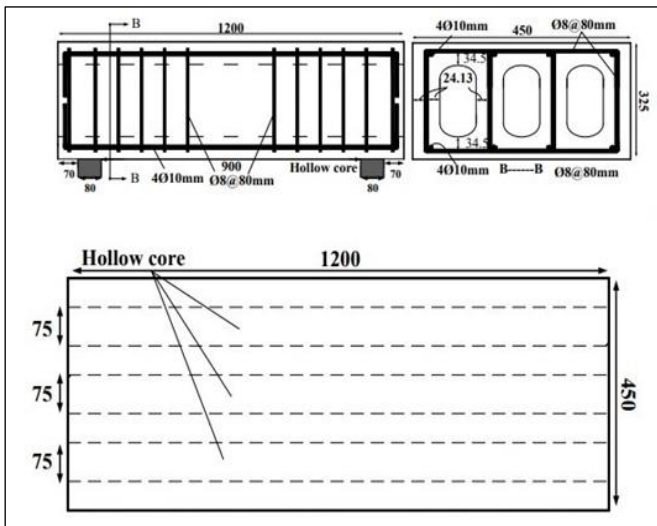


Figure 7. Actual casting mold

As illustrated in Figure 7, the hollow slab is fastened on both sides and strengthened by utilizing reinforcement steel bars measuring 8@80mm in each direction. Both the ultimate and yield strengths of the steel bars come in at 696 MPa. The hollow core model was drawn using the Solid Work program at the same dimensions as shown in Figure 8.

3.2 Research boundary conditions

The built-in models, user-defined material models, or Material Designer in Mechanical can be used to generate representative volume elements to simulate the behavior of complicated materials. Alternatively, user-defined material

models can be used. Models with extremely substantial deformation do not always need to be simplified by making an unnecessary move to explicit solvers. The nonlinear adaptive capability tackles challenging simulations automatically by reshaping the solution as the simulation moves on. The results are shown in Figure 9.

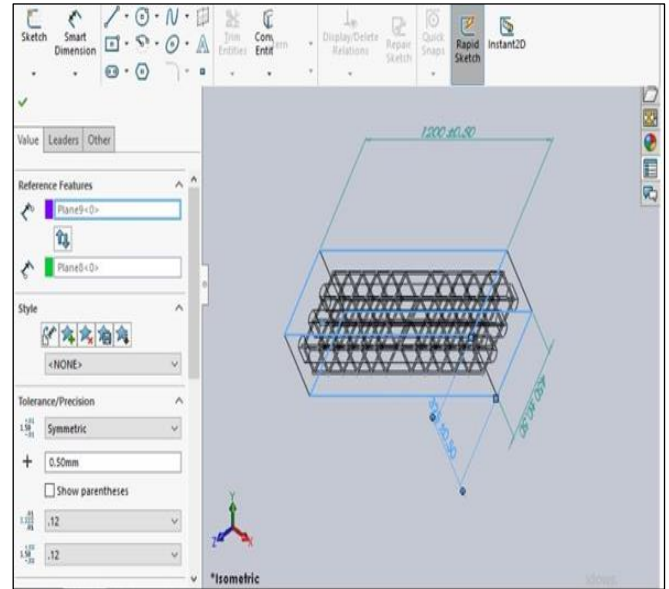


Figure 8. Results of hollow core shape plot

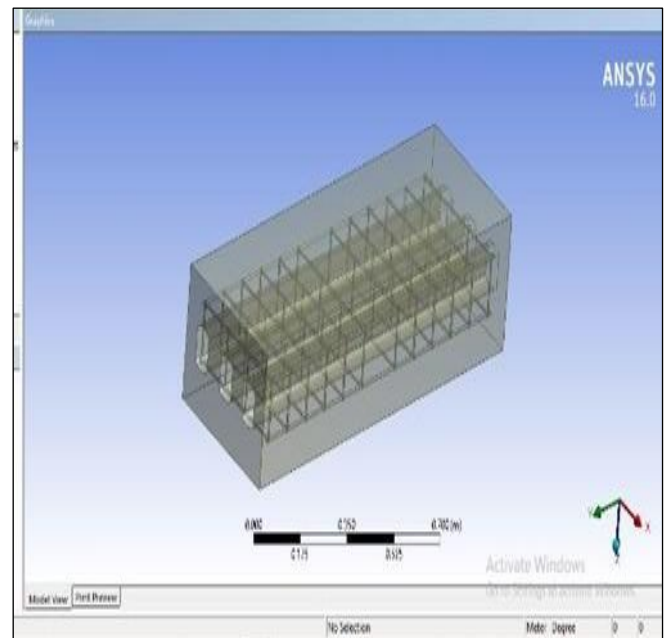


Figure 9. Reinforced hollow core results

4. RESULTS AND DISCUSSION

This section illustrates the ANSYS testing results based on the earlier boundary conditions and assumptions considered as the basis for the simulation of the hollow core slab. The models employed in this work are validated using the acquired experimental data. Additionally, it is used to choose a suitable turbulence model that can be constructed and applied to the boundary condition that we are interested in, with the proper model setup and a correct mesh technique. Doing all those

tests made it possible to understand concrete behavior based on a chosen hollow core model and observe the proper method for developing models. The validation approach is used to confirm that the structural simulation model was developed in the right conditions and will be solved in a manner that provides a good picture of reality. Figure 10 and Figure 11 illustrate the numerical deflection findings linked to non-reinforced and reinforced hollow concrete cores, respectively.

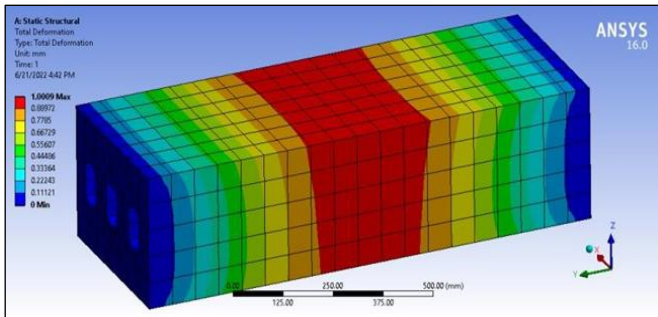


Figure 10. Non-reinforced hollow core deflection result at load 130 kN

It can be inferred from Figure 10 that total deformations in the non-reinforced hollow core of the concrete slab had a maximum value at the center of the concrete slab, corresponding to 1 mm compared to approximately zero deflection at the sides of the slab.

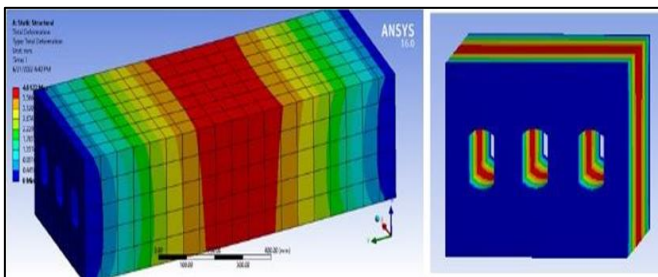


Figure 11. Reinforced hollow core deflection result at load 250 kN

It is also concluded from the numerical outputs presented in Figure 11 that the maximum deflection takes place at the center at the reinforced hollow concrete core compared to the its sides where roughly no deflection is presented. These results are close to the outputs obtained in the case represented in Figure 10.

4.1 Impact of integrating $V_f = 0.5$, SFRC

Based on the measurements provided, the first thing that must be done in hollow core modeling is to construct a volume for the concrete body. Because of the symmetry in the geometry of all of the members, the steel supports and reinforcements used in the FE analysis will be modeled as being cut in half. The typical load versus concrete displacement parameters is depicted in this section.

The load-deflection curves were calculated using the central location of the hollow slab to achieve the results [11]. The ANSYS software package evaluated the geometric changes of the hollow slab, including deflection and failure form changes under varying temperatures and load levels. In contrast to the load history advised by FEMA, the analyses with monotonic

loading were carried out by providing a monotonic vertical displacement load to the beam tip until more than 4% of total rotation was achieved at the column web center [12]. The geometric measurement of these changes was assessed and examined. Figure 12 depicts the position of the testing forces used in the simulation.

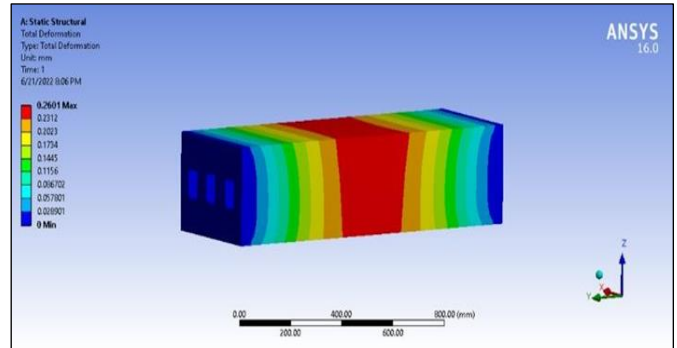


Figure 12. ANSYS results of displacement for force 50, $V=0.5$, non-reinforced concrete with SFRC

The data represented in Figure 12 explain that these measurements may be connected with the data on the load and displacement, which enables visual observations to be related to the force being applied and the distance it travels.

A comparison of the force-displacement response is provided for every hollow core model that ANSYS evaluated in these figures. The loading was applied at a range of various values from 25 to 250 kN. Figure 13 and Figure 14 represent the research findings associated with the steel-fiber reinforced concrete slab model.

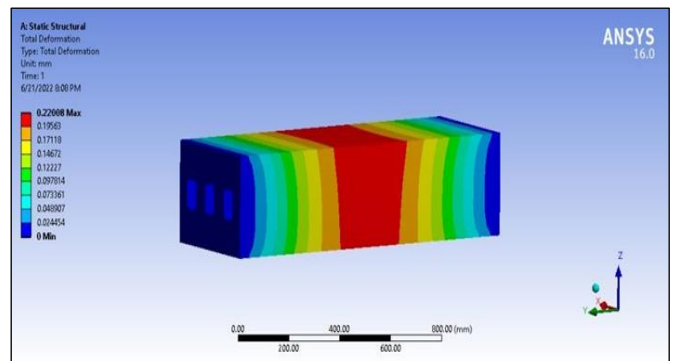


Figure 13. ANSYS results of displacement for force 50, $V=0.5$, reinforced concrete with SFRC

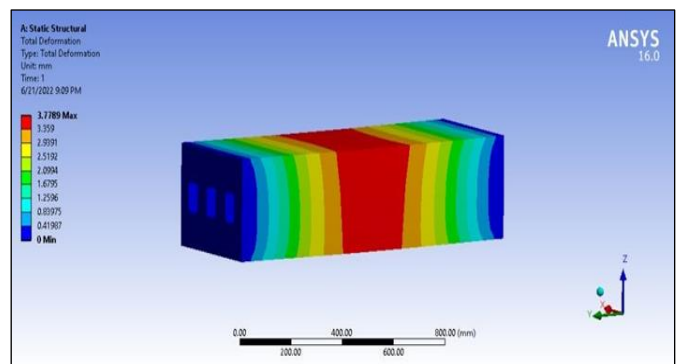


Figure 14. ANSYS results of displacement for force 250, $V=0.5$, reinforced concrete with SFRC

It can be noted from Figure 13 and Figure 14 that using SFRC has mitigated the deflection amount in concrete compared with previous cases (in which no SFRC is employed) and had a more deflection value, like the reference case (first case) that used no SFRC.

Furthermore, Figure 15 presents the findings associated with the tests that were given were utilized in the production of hollow core slabs with $V=0.5$ SFRC additives.

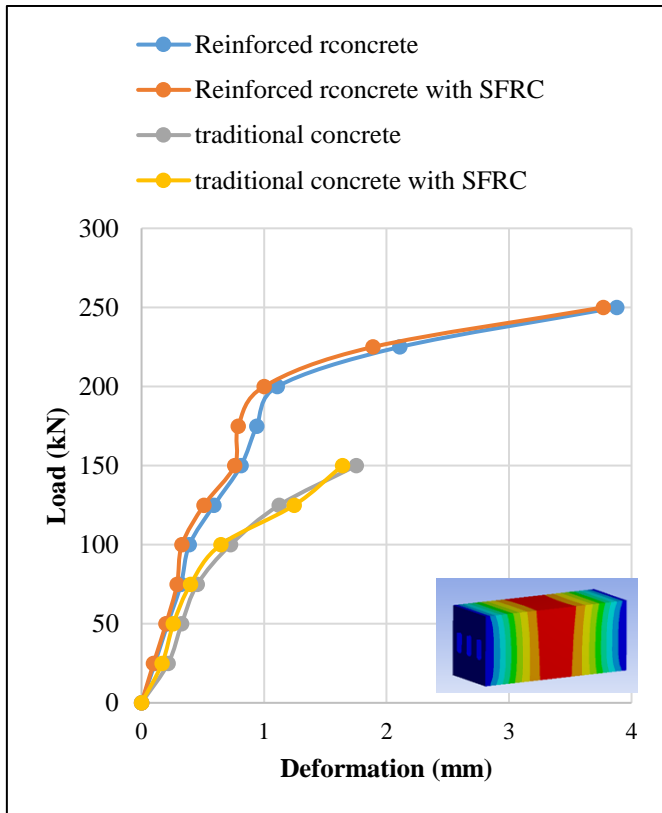


Figure 15. Plot the test results for hollow test $V=0.5$

It can be inferred from the results indicated in Figure 15 that the numerical deflection results confirmed that when the specimens are subjected to different load values, the deflection would rise linearly until it reaches a value of roughly 200 kN. At this point, the variation correlation will change. This phenomenon was observed when the compressive loading was applied to the specimen.

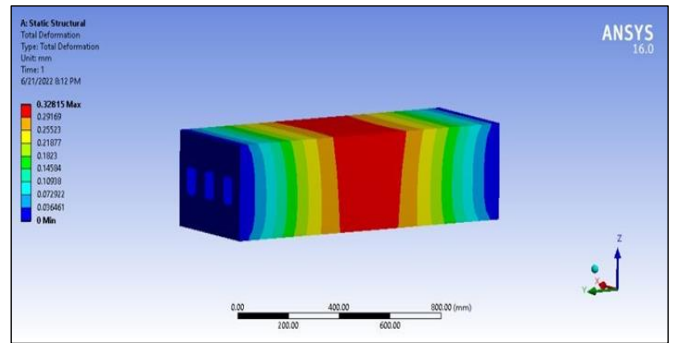
4.2 Impact of integrating $V_f = 1.0$, SFRC fibers

ANSYS performed a series of tests on the model utilizing a variety of loading conditions and exposed it to point load. The additives were defined in terms of their volume fractions and were initially tested at a concentration of 1.0. The outcomes of the behavior of the hollow slab are depicted in Figures 16 (a) to 16 (f), which represent the numerical findings associated with displacement corresponding to various values of compressive loading.

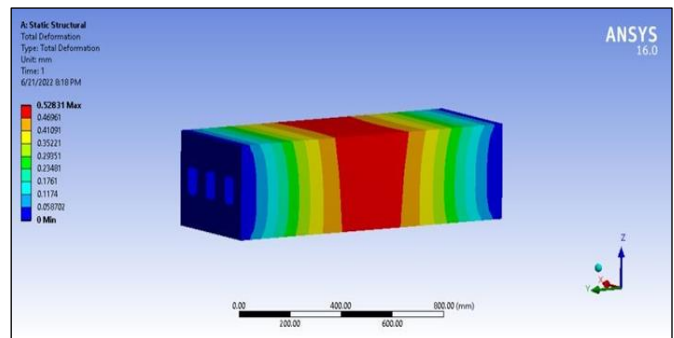
The results obtained in Figures 16 (a) and (b) can suggest that while the burning temperature is held constant, increasing the steel fiber doses would lead to a decline in the deflection values, as it can be observed in the result of the placed center load results.

According to the findings of the ANSYS tests represented in Figures d and e, it can be noted that the behavior of the results of the hollow slab with SFRC fibers is comparable to

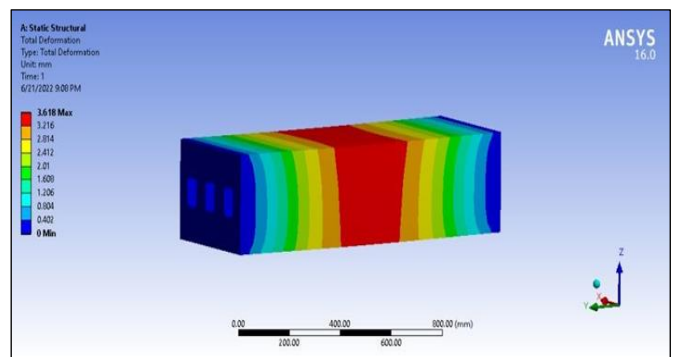
that of genuine results, which can be clearly split into two zones. Figure 16 (f) illustrates the resulting plot for your reference.



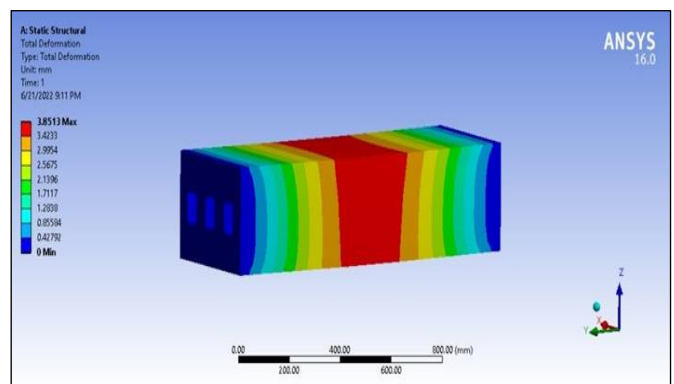
(a). ANSYS results of displacement for force 50, $V=1$



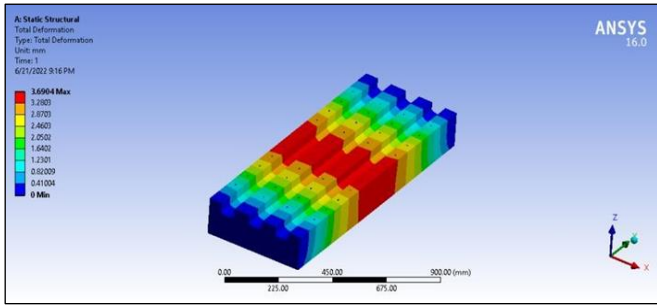
(b). ANSYS results of displacement for force 150, $V=1$, SFRC type 1



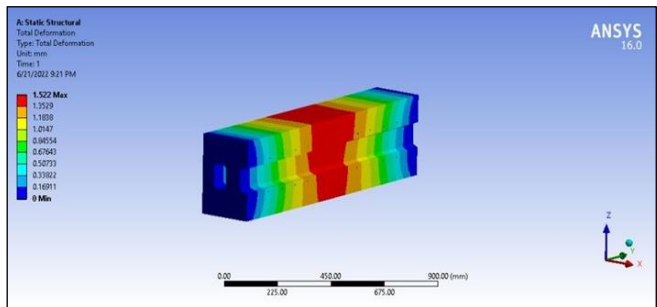
(c). ANSYS results of displacement for force 250, $V=1$, second type of SFRC



(d). ANSYS results of displacement for force 250, without additives



(e). ANSYS section results of displacement for force 250, V=1



(f). ANSYS section results of displacement for force 150, V=1

Figure 16. (a). ANSYS results of displacement for force 50, V=1; (b). ANSYS results of displacement for force 150, V=1, SFRC type1; (c). ANSYS results of displacement for force 250, V=1, second type of SFRC; (d). ANSYS results of displacement for force 250, without additives; (e). ANSYS section results of displacement for force 250, V=1; (f). ANSYS section results of displacement for force 150, V=1

From the results represented in Figure 18, it can be seen that the loads deflection responses depending on numerical ANSYS test were clear. It can be concluded that the utilization of hollow slabs reinforced with SFRC fibers led to an increase in load dependability, which in turn led to a reduction in the slab deflection that occurred under the same conditions. Hence, the findings of the tests indicate that the SFRC fibers are active, which will considerably contribute to considerable improvements. In addition, it is noted from the comparative analysis between Figure 17 and Figure 18 that using SFRC in reinforced hollow core concrete has increased the potential to withstand significant amounts of loads (250 kN) compared with non-reinforced hollow concrete core that had only a maximum load of 150 kN.

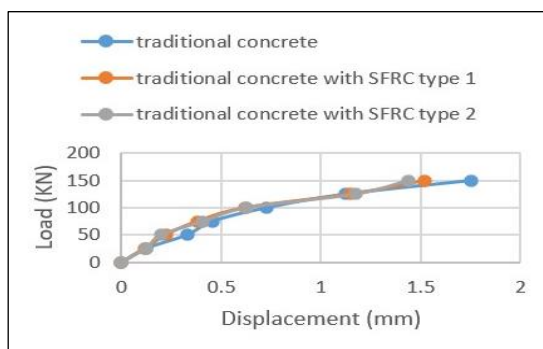


Figure 17. Results of adding different SFRC shapes to non-reinforced hollow core

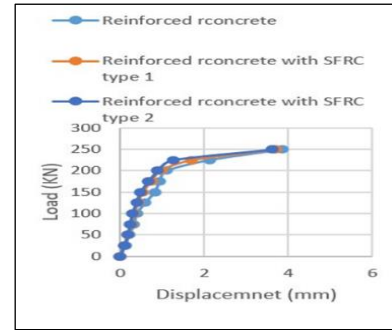


Figure 18. Results of adding different SFRC shapes to reinforce hollow core

5. CONCLUSION

Hollow-core (HC) slabs are the most widely used and economically advantageous type of precast/prestressed concrete floor system. HC slabs made for the American market have a 6-12 inch unutilized depth (152 to 305 mm). Deeper HC slabs, such as 16-inch [406 mm] slabs, have lately been developed in response to the need for longer spans and heavier loads.

The paper investigates how hollow slabs perform in terms of shear strength. Here, we investigate residual strength and the deterioration of mechanical features by use of a hollow core model. In this work, an experimental investigation into the shear resistance mechanism of hollow slabs reinforced using a core-filling technique was conducted. The number of filled seats and the shear reinforcement ratio were established as test factors, and their effects on the behavior of the specimens, the patterns and angles of fractures that emerged in the Hollow slabs units, and filled cores were analyzed in detail.

In order to process a real-world hollow slab case study, this work use the ANSYS software tool to give a set of operations and circumstances. The main contribution of this work is an investigation into the deflection behavior of hollow slab panels with different percentages of SFRC fiber reinforcement. This topic has a practical base in learning how a concrete slab reacts under different loads and to different impacts. The range of 25-250 kN was chosen as the load range of interest. It is from this work that the following inferences can be made:

- (1) The optimal displacement was obtained when the SFRC fibers had a V value of 1.5, which was based on the load effect; however, the best results gained from fiber percentage were obtained when the value was V=1 for the range of 25 to 200 kN.
- (2) Employing the first type of SFRC accomplished a considerable decline in the deflection of concrete. Deflection reduction ratios of 4.16% and 6.23% were obtained after adding the first and second types of SFRC into reinforced hollow concrete core, respectively.
- (3) Adding the first and second types of SFRC into non-reinforced hollow concrete core accomplished a reduction portion of 12.2% and 20.39%, respectively.

REFERENCES

- [1] Altemen, A.A.A.B.U., Arna'ot, F.H., Abbass, A.A., Ozakca, M. (2017). Punching shear behavior of small SFRC flat plate. ICOCEE-Cappadocia, pp. 891-901.
- [2] American Concrete Institute. (2014). ACI318, Building Code Requirements for Structural Concrete (ACI 318M-

- 14) and Commentary (ACI 318RM-14).
- [3] Al-Yassri, L.S., Ali, A.Y., AL-Khafaji, M.M. (2017). Experimental investigation for the behavior of hollow core concrete slab reinforced with hybrid reinforcement. *Al-Qadisiyah Journal for Engineering Sciences*, 10(3): 308-317.
- [4] Brunesi, E., Bolognini, D., Nascimbene, R. (2015). Evaluation of the shear capacity of precast-prestressed hollow core slabs: numerical and experimental comparisons. *Materials and Structures*, 48: 1503-1521. <https://doi.org/10.1617/s11527-014-0250-6>
- [5] Chowdhury, M.A., Hossain, S. (2020). A review on tensile and flexural properties of fiber-reinforced polymer composites. *Journal of Polymer Science Part A: Polymer Chemistry*, 7: 16-26.
- [6] Darwin, D., Dolan, C.W., Nilson, A.H. (2016). *Design of Concrete Structures (Vol. 2)*. McGraw-Hill Education New York, NY, USA.
- [7] Djodikusumo, I., Diasta, I.N., Sanjaya Awaluddin, I. (2016). Geometric Modeling of a Propeller Turbine Runner Using ANSYS BladeGen, Meshing Using ANSYS TurboGrid and Fluid Dynamic Simulation Using ANSYS Fluent. *Applied Mechanics and Materials*, 842: 164-177. <https://doi.org/10.4028/www.scientific.net/AMM.842.164>
- [8] Lindsay, R., Mander, J.B., Bull, D.K. (2004). Experiments on the seismic performance of hollow-core floor systems in precast concrete buildings. Master of Engineering Thesis.
- [9] Meng, X. (2016). Shear strengthening of prestressed hollow core slabs using externally bonded Carbon Fiber Reinforced Polymer sheets. Thesis. University of Windsor (Canada).
- [10] Nabil, A., Meleka, N., Heiza, K. (2017). Effects of different types of concrete toppings on the behavior of PPHC slabs. *ERJ. Engineering Research Journal*, 40(4): 331-339. <https://doi.org/10.21608/erjm.2017.66359>
- [11] Naimi, S., Celikag, M., Hedayat, A.A. (2013). Ductility enhancement of post-Northridge connections by multilongitudinal voids in the beam web. *The Scientific World Journal*, 2013: 515936. <https://doi.org/10.1155/2013/515936>
- [12] Naimi, S., Omar, M., Hanoun, M.A. (2018). Comparison of equivalent static analysis and mode combination method for concrete buildings according to Turkish standard. *Honorary Editor*, 8(4): 1609-1625.
- [13] Dehqan Nezhad, Y., Naimi, S. (2022). Numerical investigation of precast reinforced concrete beam-to-column joints by replaceable damper. *Journal of Sustainable Construction Materials and Technologies*, 7(2): 81-87. <https://doi.org/10.47481/jscmt.1117101>
- [14] Picazo, A., Alberti, M.G., Gálvez, J.C., Enfedaque, A. (2021). Shear slip post-cracking behaviour of polyolefin and steel fibre reinforced concrete. *Construction and Building Materials*, 290: 123187. <https://doi.org/10.1016/j.conbuildmat.2021.123187>
- [15] Ren, L., Zhang, L., Wang, Q. (2018). Measurements of surface velocity and level fluctuation in an actual continuous wide slab casting mold. *Metallurgical Research & Technology*, 115(1): 102. <https://doi.org/10.1051/metal/2017074>
- [16] Saksala, T., Mäkinen, J. (2020). Numerical modeling of cracking in gravity dam under static and seismic loadings with multiple pre-embedded discontinuity FEM. *Procedia Structural Integrity*, 28: 784-789. <https://doi.org/10.1016/j.prostr.2020.10.091>
- [17] Salomao, R., Pandolfelli, V.C. (2007). Polypropylene fibers and their effects on processing refractory castables. *International Journal of Applied Ceramic Technology*, 4(6): 496-502. <https://doi.org/10.1111/j.1744-7402.2007.02170.x>
- [18] Shoenberger, J.E., Tom, J.G. (1992). Polypropylene fibers in Portland cement concrete pavements. Army Engineer Waterways Experiment Station Vicksburg MS Geotechnical Lab, Polypropylene Fibers in Portland Cement Concrete Pavements. (dtic.mil).
- [19] Song, F. (2017). Steel fiber reinforced concrete under concentrated load. Doctoral Thesis, Ruhr University Bochum, Faculty of Civil and Environmental Engineering. <http://nbn:de:hbz:294-52050>.
- [20] Torgal, F.P., Jalali, S. (2011). Natural fiber reinforced concrete. In *Fibrous and Composite Materials for Civil Engineering Applications*, pp. 154-167. <https://doi.org/10.1533/9780857095583.2.154>
- [21] Yadav, A.K., Prasad, B., Kumar, V., Mohan, M. (2017). Properties of polypropylene fiber reinforced concrete and structural behavior of beam. *International Journal Innovative Research Science Engineering Technology*, 6(6): 10200-10210. <https://doi.org/10.15680/IJIRSET.2017.0606011>
- [22] Reihanifar, M., Naimi, S. (2016). Proje ve Maliyet Yönetimi Yöntemleriyle Kalitenin ve Verimliliğin Artırılmasının İncelenmesi. *İstanbul Aydın Üniversitesi Dergisi*, 8(29): 51-65.
- [23] Akbay, C., Naimi, S. (2021). İnşaat Projelerinde Proje Yönetim Tekniklerinin Kullanılması: Aksaray Mahmudiye Ortaokulu Örneği. *MAS Journal of Applied Sciences*, 6(3): 743-753. <https://doi.org/10.52520/masjaps.104>
- [24] Yousefi, M., Khandestani, R., Gharaei-Moghaddam, N. (2022). Flexural behavior of reinforced concrete beams made of normal and polypropylene fiber-reinforced concrete containing date palm leaf ash. *Structures*, 37: 1053-106. <https://doi.org/10.1016/j.istruc.2022.01.067>
- [25] Li, Y., Zhang, J., He, Y., Huang, G., Li, J., Niu, Z., Gao, B. (2022). A review on durability of basalt fiber reinforced concrete. *Composites Science and Technology*, 225: 109519. <https://doi.org/10.1016/j.compscitech.2022.109519>
- [26] Palanisamy, E., Ramasamy, M. (2022). Dependency of sisal and banana fiber on mechanical and durability properties of polypropylene hybrid fiber reinforced concrete. *Journal of Natural Fibers*, 19(8): 3147-3157. <https://doi.org/10.1080/15440478.2020.1840477>
- [27] Deng, F., Cao, C., Xu, L., Chi, Y. (2022). Interfacial bond characteristics of polypropylene fiber in steel/polypropylene blended fiber reinforced cementitious composite. *Construction and Building Materials*, 341: 127897. <https://doi.org/10.1016/j.conbuildmat.2022.127897>
- [28] Wang, J., Dai, Q., Si, R., Guo, S. (2019). Mechanical, durability, and microstructural properties of macro synthetic polypropylene (PP) fiber-reinforced rubber concrete. *Journal of Cleaner Production*, 234: 1351-1364. <https://doi.org/10.1016/j.jclepro.2019.06.272>
- [29] Yan, X., Wan, D., Hu, D., Han, X., Liu, G.R. (2022). A selective smoothed finite element method for 3D explicit

dynamic analysis of the human annulus fibrosus with modified composite-based constitutive model. *Engineering Analysis with Boundary Elements*, 134: 49-65. <https://doi.org/10.1016/j.enganabound.2021.09.021>

[30] Stephen, C., Thekkuden, D.T., Mourad, A.H.I., Shivamurthy, B., Selvam, R., Behara, S.R. (2022). Prediction of impact performance of fiber reinforced polymer composites using finite element analysis and artificial neural network. *Journal of the Brazilian Society of Mechanical Sciences and Engineering*, 44(9): 408. <https://doi.org/10.1007/s40430-022-03711-8>

[31] Kawagoe, Y., Kawai, K., Kumagai, Y., Shirasu, K., Kikugawa, G., Okabe, T. (2022). Multiscale modeling of process-induced residual deformation on carbon-fiber-reinforced plastic laminate from quantum calculation to laminate scale finite-element analysis. *Mechanics of Materials*, 170: 104332. <https://doi.org/10.1016/j.mechmat.2022.104332>

[32] Gopinath, G., Batra, R.C. (2022). Finite element method based micromechanical methodology for homogenizing fiber/fabrics-reinforced composites and their progressive failure. *Composite Structures*, 286: 115279. <https://doi.org/10.1016/j.compstruct.2022.115279>

[33] Solahuddin, B.A. (2022). A critical review on experimental investigation and finite element analysis on structural performance of kenaf fibre reinforced concrete. *Structures*, 35: 1030-1061. <https://doi.org/10.1016/j.istruc.2021.11.056>

NOMENCLATURE

FE	Finite Element
RC	Reinforced Concrete

Greek symbols

d'	Depth of compressive reinforcement
------	------------------------------------

EC	Modulus of elasticity for concrete
ES	Modulus of elasticity for steel plates
AV	Area of stirrups legs
f_c'	Compressive strength of concrete
ν	Poisson's ratio
ν_s	Poisson's ratio of steel
ν_c	Poisson's ratio of concrete
f_r	Modulus of rupture
$LINK180$	3D-SPAR element 2-nodes discrete element (3 DOF per node)
$SOLID185$	8-nodes brick element (3 DOF per node) (3 Translation DOF per node)
f_t	Uniaxial tensile strength for concrete
f_y	Yield stress of steel
h	Height of beam
X, Y, Z	Global coordinate system
δ	Displacement
ϵ	Strain at stress f_c
ϵ_y	Yield strain of steel
ϕ	Diameter of reinforcement bar (mm)
F	Function of principal stress state ($\sigma_{xp}, \sigma_{yp}, \sigma_{zp}$)
f_{cb}	Ultimate biaxial compressive strength.
f_s	The steel stress
f_1	Ultimate compressive strength for a state of biaxial compression superimposed on hydrostatic stress state (σ_{ha}) superimposed on hydrostatic stress state (σ_{ha})
f_2	Ultimate compressive strength for a state of uniaxial compression superimposed on hydrostatic stress state (σ_{ha})
f_n	Stress normal to the crack plane
ϵ_n	Strain normal to the crack plane
E_i	The secant modulus